Acta Crystallographica Section B
Structural Science
ISSN 0108-7681

The effect of pressure on the crystal structure of bianthrone

Russell D. L. Johnstone,[a] David Allan,[b] Alistair Lennie,[b] Elna Pidcock,[c] Rafael Valiente,[d] Fernando Rodríguez,[e] Jesús Gonzalez,[e] John Warren[f] and Simon Parsons[a]*

[a]School of Chemistry and Centre for Science at Extreme Conditions, The University of Edinburgh, King's Buildings, West Mains Road, Edinburgh EH9 3JJ, Scotland, [b]Diamond Light Source Ltd, Diamond House, Harwell Science and Innovation Campus, Didcot, Oxfordshire OX11 0DE, England, [c]Cambridge Crystallographic Data Centre, 12 Union Road, Cambridge CB2 1EZ, England, [d]MALTA-Consolider Team, Dpt. Física Aplicada, Facultad de Ciencias, Universidad de Cantabria, Santander 39005, Spain, [e]MALTA-Consolider Team, DCITIMAC, Facultad de Ciencias, Universidad de Cantabria, Santander 39005, Spain, and [f]Department of Chemistry, University of Liverpool, Crown Street, Liverpool L69 7ZD, England

Correspondence e-mail: s.parsons@ed.ac.uk

Received 1 September 2010
Accepted 14 March 2011

Bianthrone [10(10-oxoanthracen-9-ylidene)anthracen-9-one] consists of two tricyclic anthraceneone units connected by a carbon–carbon double bond. Crystals of the form obtained under ambient conditions are yellow and contain folded centrosymmetric conformers in which the central ring of the anthraceneone unit is non-planar. When hydrostatic pressure is applied the crystals assume a red colouration which gradually deepens as pressures increases. The colour change is limited in extent to the surface of the crystals, the bulk remaining yellow. Comparison of high-pressure, single-crystal UV–vis spectra and powder diffraction data demonstrate that the colour change is associated with the formation of a polymorph containing a conformer in which the tricyclic fragments are planar and the molecule is twisted about the central C—C bond. Single-crystal diffraction data collected as a function of pressure up to 6.5 GPa reveal the effect of compression on the yellow form, which consists of layers of molecules which stack along the [010] direction. The structure remains in a compressed form of the ambient-pressure phase when subjected to hydrostatic pressure up to 6.5 GPa, and the most prominent effect of pressure is to push the layers closer together. PIXEL calculations show that considerable strain builds up in the crystal as pressure is increased with a number of intermolecular contacts being pushed into destabilizing regions of their potentials.

1. Introduction

Bianthrone [10(10-oxoanthracen-9-ylidene)anthracen-9-one] is part of a family of compounds which are known as *bistricyclic aromatic enes* (BAEs). Crystals of bianthrone are bright yellow and the molecules adopt a 'folded' conformation (Fig. 1*a*; Harnik & Schmidt, 1954). In solution bianthrone changes colour reversibly from bright yellow to dark green when subjected to heat (thermochromism; Meyer, 1909*a*,*b*) or light (photochromism; Kortum, 1974). Yellow crystals of bianthrone are neither photochromic nor thermochromic; however, they are reported to change colour to dark green on grinding with a pestle and mortar (Wasserman & Davies, 1959). The same molecular species is responsible for the green colour of the forms obtained under all three sets of conditions, and is associated with an absorption band at $\sim$ 650 nm in the UV–vis spectrum. The green form reverts slowly back to the yellow form over time (Fanselow & Drickamer, 1974).

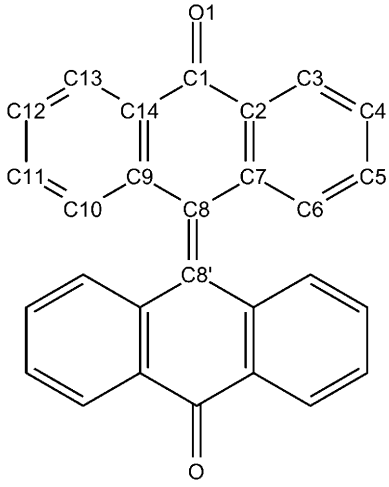

While thermo-, photo- and piezochromism are properties common to many BAEs, the structures of the deeply coloured forms have been debated for over a century. Relatively recently, however, Biedermann *et al.* (2006) obtained the crystal structures of two polymorphic forms of one BAE, 9-(2,7-dimethyl-9*H*-fluoren-9-ylidene)-9*H*-xanthene. Sublimation of this compound yielded yellow and purple polymorphs in different zones of the sublimation apparatus. The yellow form contained molecules in a folded conformation analogous to that of the yellow form of bianthrone. The purple crystals contained molecules in a twisted conformation in which the two tricyclic moieties were essentially planar, but with a dihedral angle of 50.1° about the linking C—C bond. This structure is reminiscent of a structure for the green form of bianthrone (Fig. 1*b*) with a twist angle of 55° that had been suggested by Korenstein *et al.* (1973) on the basis of proton NMR spectroscopy and minimum energy strain calculations.

The behaviour of bianthrone in the solid state with pressure was studied by Fanselow & Drickamer (1974), who dispersed the compound in a solid polymer, polymethylmethacrylate, and then collected UV–vis spectra up to around 12 GPa. Fanselow and Drickamer do not refer to 'yellow' or 'green' forms in their paper, preferring instead to refer to them as 'A' and 'B' forms, perhaps because the dispersion used was dilute, 0.0003–0.0006 mol mol^{-1} of methylmethacrylate monomer, and the sample sizes necessarily tiny. However, the spectra obtained contained one band due to the yellow '*A*' form at between 400 and 465 nm (depending on the pressure) which decreased in intensity with pressure and another due to the green '*B*' form at 650 nm which appeared and then increased in intensity as pressure was increased. At the highest pressure reached the conversion to the green form was 30%.

The aim of the present study was to investigate the behaviour of bianthrone at high pressure using single-crystal X-ray diffraction. One aim of the study was to show whether the colour change that is observed in bianthrone upon grinding could be reproduced by the application of hydrostatic pressure to a single crystal in a diamond–anvil cell. Although Fanselow and Drickamer's results showed that it was unlikely that we would observe complete conversion to the green form under

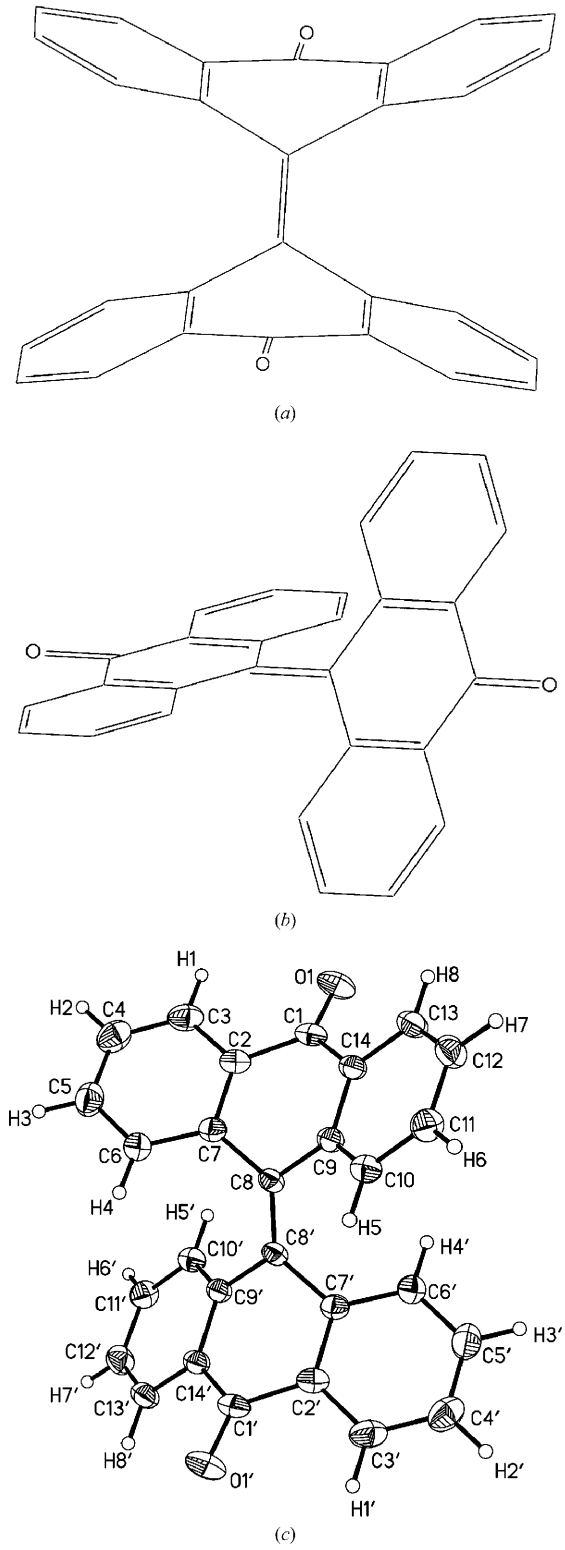

Figure 1
(*a*) The ambient temperature/pressure, 'folded' conformation of bianthrone (Harnik & Schmidt, 1954). (*b*) The proposed twisted form (Harnik, 1956; Korenstein *et al.*, 1973). (*c*) Molecular structure of bianthrone derived from the crystal structure at ambient pressure. Ellipsoids enclose 30% probability surfaces. Primed atoms are related to unprimed atoms by the operation $(2 - x, 1 - y, 1 - z)$.

Table 1
Crystallographic data for bianthrone at ambient pressure and 6.5 GPa pressures.

For all structures: $C_{28}H_{16}O_2$, M_r = 384.43, monoclinic, $P2_1/n$, Z = 2. Experiments were carried out at 293 K. Absorption was corrected for by multi-scan methods, *SADABS* (Sheldrick, 2008). Refinement was on 136 parameters. H-atom parameters were constrained. Data for all pressures are available in the supplementary material (Table S1).

	Ambient pressure	6.5 GPa
Crystal data		
a, b, c (Å)	10.1860 (3), 8.4277 (2), 11.6457 (3)	9.7119 (14), 7.041 (2), 11.2282 (18)
β (°)	109.591 (2)	110.229 (10)
V (Å^3)	941.85 (4)	720.4 (3)
Radiation type	Mo $K\alpha$	Synchrotron, λ = 0.47920 Å
μ (mm^{-1})	0.08	0.11
Crystal size (mm)	0.57 × 0.33 × 0.31	0.20 × 0.20 × 0.10
Data collection		
Diffractometer	Area	Area
T_{min}, T_{max}	0.82, 0.97	0.81, 0.99
No. of measured, independent and observed [$I > 2.0\sigma(I)$] reflections	12 386, 2349, 1867	3016, 641, 473
R_{int}	0.049	0.117
d_{max}, d_{min} (Å^{-1})	8.84, 0.75	5.95, 0.90
θ_{max} (°)	28.3	15.1
Refinement		
$R[F^2 > 2\sigma(F^2)]$, $wR(F^2)$, S	0.055, 0.051, 1.11	0.051, 0.039, 1.09
No. of reflections	1867	473
No. of restraints	0	187
$\Delta\rho_{max}$, $\Delta\rho_{min}$ (e Å^{-3})	0.24, −0.19	0.19, −0.19
Completeness	99.8% (0.75 Å)	67.3% (0.9 Å)

these conditions, we were interested in whether there were any features of the crystal structure of the yellow form which might hint at reasons for its instability towards compression.

Somewhat to our surprise, compression caused the crystals to become not green but red, a transition which we have further investigated using single-crystal high-pressure UV–vis spectroscopy.

2. Experimental

2.1. Crystal growth

Bianthrone was purchased from Sigma–Aldrich (Catalogue number R750077). A sample (50 mg) was dissolved in dichloromethane (5 ml). Evaporation over the course of 2 weeks at room temperature resulted in the formation of small yellow crystals on the side of the vial.

2.2. Determination of the ambient-pressure structure of bianthrone

Data were measured on a Bruker SMART APEX diffractometer with graphite-monochromated Mo $K\alpha$ radiation (λ = 0.71073 Å) at 293 K. The crystal structure of bianthrone has previously been investigated at 220 and 113 K (Parsons *et al.*, 2004; Wolstenholme & Cameron, 2006). Data were collected at room temperature to facilitate comparisons with the high-pressure data (see below), which were collected at the same temperature. The data were integrated using *SAINT* (Bruker–Nonius, 2006) and corrected for absorption with *SADABS* (Sheldrick, 2008). The structure was solved using direct methods (*SIR*92; Altomare *et al.*, 1994) and refined against F using data with $F > 4\sigma(F)$ in *CRYSTALS* (Betteridge *et al.*, 2003). All non-H atoms were refined with anisotropic displacement parameters. H atoms attached to carbon were placed geometrically and constrained to ride on their host atoms. Crystal and refinement data are given in Table 1.[1]

2.3. High-pressure crystallography: general procedures

High-pressure experiments were carried out using a Merrill–Bassett diamond–anvil cell (half-opening angle 40°), equipped with Boehler–Almax cut diamonds with 600 µm culets and a tungsten gasket with a hole diameter of 300 µm (Merrill & Bassett, 1974; Moggach *et al.*, 2008). A 4:1 mixture of methanol and ethanol was used as a hydrostatic medium. A small ruby chip was also loaded into the cell, and the ruby fluorescence method used to measure the pressure (Piermarini *et al.*, 1975).

2.4. Colour changes in single crystals of bianthrone up to 7.5 GPa

Four small crystals of bianthrone were loaded into a diamond–anvil cell. The unit-cell dimensions of each crystal were checked using single-crystal diffraction data collected at 200 K before loading in the cell, confirming each crystal to be bianthrone in its known phase. Before compression the crystals were yellow. Pressure was then increased gradually to 7.5 GPa. The colour of the crystals deepened to dark red over the course of compression (Fig. 2). The pressure was then released and the crystals recovered. Although the crystals still appeared red, on closer microscopic inspection the colour seemed to be due to a surface colouration and the bulk crystal was yellow. One of the crystals was mounted on a fibre and enough single-crystal diffraction data were collected to determine the unit-cell dimensions. These data were collected at room temperature with synchrotron radiation at (λ = 0.5159 Å) on Beamline I19 at Diamond Light Source using a Crystal Logic four-circle κ-geometry goniometer and a Rigaku Saturn 724 CCD detector. The unit-cell dimensions determined were a = 10.181 (9), b = 8.487 (10) c = 11.679 (7) Å, β = 109.58 (6)° for a primitive monoclinic cell and 127 reflections.

[1] Supplementary data for this paper are available from the IUCr electronic archives (Reference: GW5012). Services for accessing these data are described at the back of the journal.

2.5. Compression of bianthrone studied by UV–vis spectroscopy

Pressure-dependent absorption spectra were obtained in a membrane diamond–anvil cell (DAC) with silicon oil as the pressure transmitter equipped with a steel gasket of diameter 200 μm and estimated thickness 50 μm. Spectroscopic paraffin oil was used as a transmitting medium. Spectra were collected in a locally constructed single-beam setup. The procedure was as follows: the modulated light (chopped with a frequency controller SR-540) of a tungsten lamp was focused on the sample with a reflection microscope objective. The transmitted light was collected with another reflection microscope objective and detected synchronously (lock-in SR-830) using a 0.5 m monochromator (Chromex IS500) equipped with a R928 photomultiplier detector (Hamamatsu). Ruby chips were used for pressure calibration and verification of hydrostatic conditions, as in the single-crystal work described above. The spectra were collected at room temperature between ambient pressure and 8.1 GPa (Fig. 3*a*).

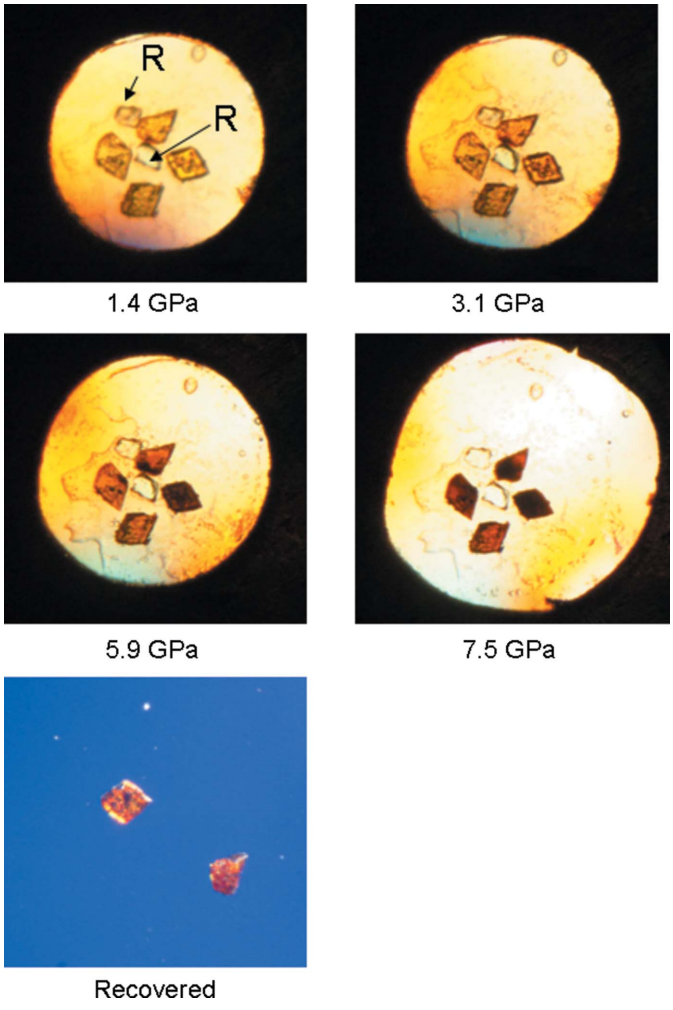

Figure 2
Colour changes in four single crystals of bianthrone as a function of pressure. The first four images were taken with the crystals inside a diamond–anvil cell; the fragments labelled '*R*' in the 1.4 GPa image are ruby chips used for pressure measurement. The gasket hole is much larger in the 7.5 GPa image because the gasket was beginning to fail (note the crack appearing at the top right). The last image shows two of the crystals as recovered from the cell: this image is only partially successful in showing that the remaining red colouration is due to a surface effect while the bulk of the crystal was yellow – the effect was rather more convincing in the original microscope images. A third crystal was used for data collection, but the forth adhered to the inner wall of the gasket during downloading and was not recovered.

2.6. High-pressure single-crystal diffraction study of bianthrone up to 6.5 GPa

All diffraction data were collected on a Bruker–Nonius APEX-II diffractometer with silicon-monochromated synchrotron radiation (λ = 0.4780 Å) on Station 9.8 at the SRS, Daresbury Laboratory. Data collection and processing procedures for all high-pressure experiments were similar to those described by Dawson *et al.* (2004). Integrations were carried out using dynamic masking of the regions of the detector shaded by the pressure cell with the program *SAINT*. Absorption and gasket-shading corrections were carried out with the program *SADABS*. Data were merged using *SORTAV* (Blessing, 1987).

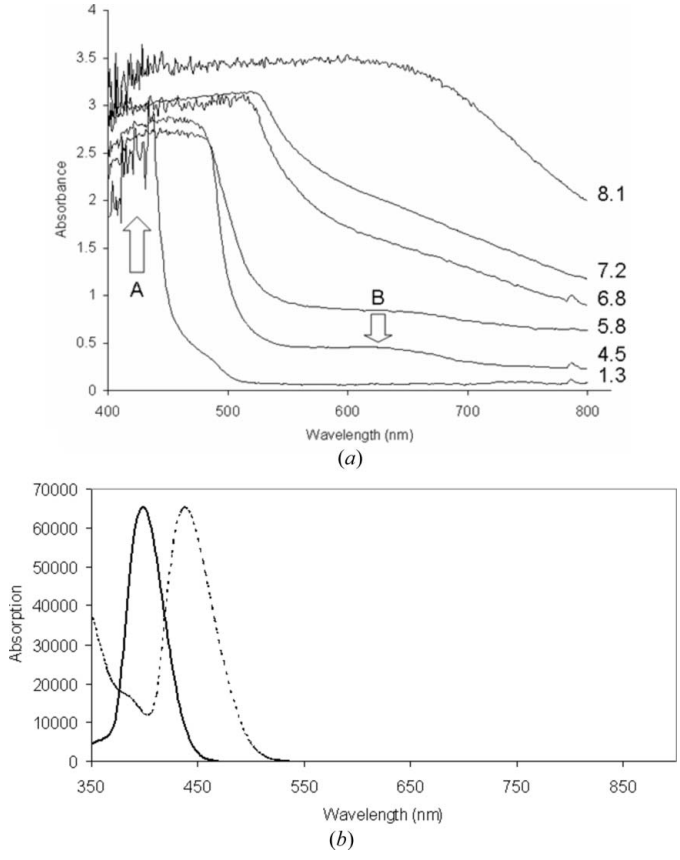

Figure 3
(*a*) Experimental UV–vis spectra of bianthrone measured as a function of pressure, listed on the far right in GPa. The bands labelled '*A*' and '*B*' are discussed in the text. (*b*) Calculated spectra of the yellow phase of bianthrone containing the folded conformation of the molecule. The spectra were calculated using *CASTEP* on the basis of geometry optimizations of the ambient-pressure and 6.5 GPa crystal structures using plane-wave DFT. The ambient-pressure spectrum is shown as a full line, the 6.5 GPa spectrum as a dotted line.

Refinements of the compressed form of bianthrone were carried out starting from the coordinates determined at ambient pressure. Refinement procedures followed those at ambient conditions, although owing to the low completeness of the data sets all primary bond distances and angles were restrained to the values observed at ambient conditions. All non-H atoms were refined with anisotropic displacement parameters, with global rigid-bond and rigid-body restraints. Refinement statistics for the 6.5 GPa structure determination are given in Table 1, data for all pressures studied are available in the supplementary material.

Above 6.5 GPa the diffraction peaks became very broad and no useful data could be obtained.

2.7. High-pressure powder diffraction study of bianthrone up to 9.6 GPa

A polycrystalline sample of bianthrone was lightly ground in a slurry of a 4:1 mixture of methanol and ethanol and loaded into a diamond–anvil cell of the type described above using the same hydrostatic medium. Diffraction data were collected with 70 s exposures on beamline I11 at Diamond Light Source. The sample was oscillated through $\pm5^\circ$ about the direct beam direction during data collection. The diffraction pattern was detected using a Mar 345 image plate and integrated using *FIT2D* (Hammersley, 1997). Data were collected between 1.3 and 9.6 GPa. The patterns are shown in Fig. 4.

2.8. PIXEL calculations

The final single-crystal structures obtained were used to calculate the molecular electron densities of the bianthrone molecules at each pressure using the program *GAUSSIAN*03 (Frisch *et al.*, 2004) with the MP2/6-31G** basis set. H-atom distances were set to standard neutron values in all calculations (C—H = 1.083 Å). The electron density was used to evaluate packing energies using the PIXEL method as implemented in the program *OPiX* (Gavezzotti, 2003). The output from these calculations yields a total packing energy and a breakdown into component interactions. Each energy is further broken down into its Coulombic (electrostatic), polarization, dispersion and repulsion contributions (Gavezzotti, 2005, 2007).

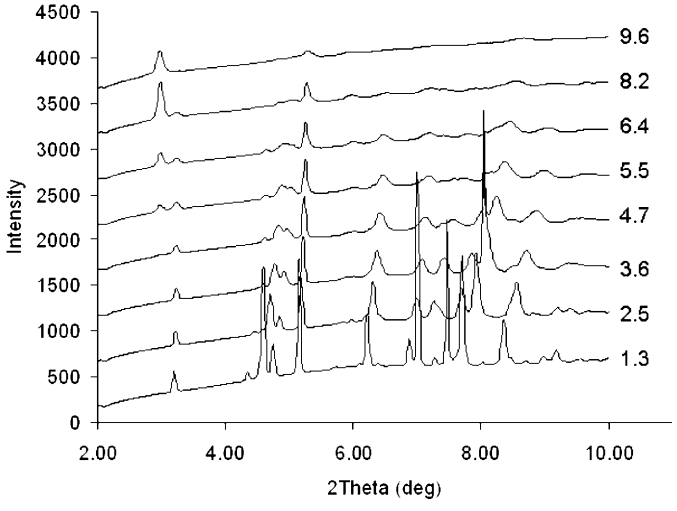

Figure 4
Powder diffraction patterns of bianthrone as a function of pressure. Pressures (in GPa) are listed on the far right of the figure.

2.9. Periodic DFT calculations

Density functional theory (DFT) calculations were performed on the ambient pressure and 6.5 GPa structures using the plane-wave pseudopotential method as implemented in the CASTEP code (Clark *et al.*, 2005). Input files were set-up and the results analysed using Materials Studio. The PBE exchange–correlation functional (Perdew *et al.*, 1996) was used with Vanderbilt ultra-soft pseudopotentials (Vanderbilt, 1990) and a basis set cut-off energy of 400 eV. Brillouin zone integrations are performed on a symmetrized Monkhorst–Pack **k**-point grid of dimensions $2 \times 2 \times 2$ (Monkhorst & Pack, 1976). These parameters yielded an energy convergence in the region of 1 meV per atom. The starting point for geometry optimization was the model from the experimental crystallographic refinements. The unit cell and space group were held fixed, but all coordinates allowed to optimize. For the geometry optimization the total energy convergence tolerance was 10^{-5} eV per atom, with a maximum force tolerance of 0.03 eV Å^{-1}, a maximum displacement of 0.001 Å and a maximum stress tolerance of 0.05 GPa. Overall the agreement between the optimized and experimental structures was excellent, with r.m.s. deviations in position over a cluster of 15 molecules being 0.015 and 0.017 Å for the ambient and 6.5 GPa structures, respectively, as calculated with the program *Mercury* (Macrae *et al.*, 2008). The optimized structures were then used to calculate the absorption spectra assuming a polycrystalline sample (Fig. 3*b*). Optical matrix element calculations were performed using a $2 \times 2 \times 2$ Monkhorst–Pack grid; use of a finer grid than this did not change the calculated absorption spectra in the region of interest (300–1000 nm). A *scissors operator* of 0.8 eV was used to adapt the results to account for underestimation of the band gap.

2.10. Other programs used

Crystal structures were visualized using the programs *CAMERON* (Watkin *et al.*, 1993), *XP* (Sheldrick, 2001), *Mercury*2.2 (Macrae *et al.*, 2008) and *DIAMOND* (Brandenburg & Putz, 2005). Analyses were carried out using *PLATON* (Spek, 2003), as incorporated in the *WIN-GX* suite (Farrugia, 1999). Ring puckering and strain calculations were carried out using *PUCKER* (Gould *et al.*, 1995) and *STRAIN* (Parsons, 2003), the latter using the JACOBI routine in Numerical Recipes (Press *et al.*, 1992). Searches of the Cambridge Structural Database utilized the program *ConQuest* with database updates up to November 2008 (Allen, 2002). Hirshfeld surface calculations were carried out with *CrystalExplorer* (McKinnon *et al.*, 2004; Wolff *et al.*, 2005). Equation of state parameters were determined with *EOSFIT* (Angel, 2002).

3. Results

3.1. Piezochromism and high-pressure UV–vis spectroscopy

Crystals of bianthrone gradually change in colour from yellow at ambient pressure to deep red at pressures above 6 GPa (Fig. 2). Samples appear to be black at 8 GPa. The crystals retain their red colouration after returning to ambient pressure. Although this colour gradually faded over time, some darkening still remained even after 3 months.

As we will show below, the single-crystal X-ray diffraction data obtained from the sample, even in its red form at 6 GPa, could be modelled as a compressed version of the starting (yellow) phase containing the folded molecules shown in Fig. 1(*a*). In addition, when one of the red crystals shown in Fig. 2 was returned to ambient pressure and diffraction data were collected, the unit-cell dimensions were the same as had been obtained for the same crystal prior to compression.

It was clear on inspecting the crystals under a microscope after removal from the pressure cell that the red colouration was restricted to grains adhering to the surfaces of the crystals, the bulk of the crystal underneath the surface covering being yellow. The diffraction patterns obtained at high and ambient pressures and the results of visual observations point to the colour change shown in Fig. 2 being a surface effect, and not the result of a phase change in the bulk sample.

More complete conversion was observed when bianthrone was studied using powder diffraction to 9.6 GPa (Fig. 4). Although peak broadening is substantial even at 2.5 GPa, there is clear evidence of a phase transition in the region around $2\theta = 3^\circ$ at 5.5 GPa, with a low-angle peak beginning to grow in. The intensity of this peak increases with pressure, the sample being mixed phase up to 8.2 GPa. The transition is essentially complete at 9.6 GPa.

While in our experiments with single crystals the colour change observed was from yellow to red, all previous publications have referred to the form obtained on grinding or compression as being green. UV–vis spectra were therefore recorded on a crystal of bianthrone as a function pressure to characterize the absorption properties of the crystals more precisely. The results are shown in Fig. 3(*a*). An intense absorption band below 450 nm (labelled '*A*' in Fig. 3*a*) moved to longer wavelength (*i.e.* red-shifted) and became broader with increasing pressure. Additionally a new broad band between 600 and 700 nm (labelled '*B*') begins to grow in above 4 GPa, increasing in intensity markedly between 5.8 and 6.8 GPa. The new band was found to persist after release of pressure.

The spectra shown in Fig. 3(*a*) are consistent with those shown in Fig. 3 in Fanselow & Drickamer (1974). The latter spectra are sharper and more clearly defined because the sample used was much more dilute, being dispersed in an inert polymer matrix (see §1). In both sets of spectra the intense absorption below 450 nm moves to longer wavelength as pressure increases. This absorption band is due to the folded (yellow) form of bianthrone, and has been assigned as a π to π^* transition. Absorption spectra calculated on the basis of DFT-optimized crystal structures at ambient pressure and 6.5 GPa (the highest pressure for which single-crystal diffraction data were colleted) are shown in Fig. 3(*b*). The calculated shift in the position of the absorption maximum by some 47 nm is consistent with the shift of 43 nm estimated from the spectra shown in Fanselow and Drickamer's paper. The absence of any predicted absorption bands between 600 and 700 nm shows that the band in this region, which is observed experimentally, is due to the formation of a new species rather than, say, perturbation of the electronic structure of the ambient-pressure phase of bianthrone as the result of short intermolecular interactions.

The absorption due to the new species being formed is at 650 nm in Fanselow and Drickamer's spectra and between 600 and 700 nm in our spectra, pointing to the formation of the same species in both studies. The transition was also incomplete in both studies: at 6.5 GPa only $\sim 10\%$ of Fanselow and Drickamer's sample had converted to the twisted form.

Absorption at around 650 nm is characteristic of the green twisted form of bianthrone, so why do the crystals in Fig. 2 appear to be red? The answer to this question lies in the positions and widths of the bands shown in Fig. 3(*a*). The band below 450 nm (labelled *A*) become red-shifted with pressure, while above 4 GPa a new band (*B*) at around 650 nm emerges. Both of these bands are broad in the single-crystal sample leading to substantial overlap in the region between 500 and 600 nm. This leads to the absorption of green light in the single crystal, and the red colour is due to reflection of light in the window of wavelengths longer than 650 nm. The bands in the spectra shown in Fig. 3 of Fanselow and Drickamer's paper are narrower with no overlap in the 500–600 nm region, which would account for the onset of the green colouration with pressure seen in previous studies.

At the highest pressures reached in the UV–vis study reported here the sample absorbs strongly at all frequencies, and this is why it then appears to be black.

3.2. The crystal structure of bianthrone at ambient pressure

Bianthrone crystallizes in the space group $P2_1/n$ with half a molecule in the asymmetric unit; the crystallographic inversion centre lies at the mid-point of the C═C bond connecting the two tricyclic moieties. At ambient temperature and pressure each molecule adopts a 'folded' conformation (Fig. 1*c*), where the two central six-membered rings take on a boat-like conformation [τ(C8′—C8—C9—C10) = 44.4 (2)° and τ(C8′—C8—C9—C14) = 137.2 (2)°]. The tricyclic groups are non-planar: a least-squares mean plane calculated using C atoms 1–14 shows that the average deviation of these atoms from the plane is 0.37 Å.

Table 2 gives the energies of the five energetically most significant (> 2 kJ mol^{-1}) intermolecular interactions in bianthrone calculated at ambient conditions. The PIXEL method calculates molecule–molecule intermolecular energies and therefore some interactions comprise more than one atom–atom contact. The geometrical parameters for each contact are also included in Table 2. The *ab initio* calculations used to obtain the electron densities employed in the PIXEL calcu-

Table 2
The main non-covalent interactions for the crystal structure of bianthrone at ambient pressure and 6.5 GPa.

Data for all pressures are available in Table S2 in the supplementary material. Distances are in Å and angles are given in °. Interactions involving rings are measured from the centroid of the ring. Hydrogen distances are not normalized to standard neutron values.

Pressure (GPa)	0	6.5
Interaction #1 (inter-layer)		
C11H6···O1^{i}		
H6···O1	2.59	2.23
C11···O1	3.309 (2)	2.750 (5)
∠C11H6O1	133	113
C10H5···*R*1^{i}		
H5···*R*2	3.75	3.53
C10···*R*2	4.624 (3)	4.363 (5)
∠C10H5*R*2	155	148
*R*2···*R*1^{ii}		
*R*2···*R*1	4.367 (1)	3.642 (3)
Offset	2.114	1.345
C4H2···*R*3^{iii}		
H2···*R*3	3.07	2.70
C4···*R*3	3.489 (3)	2.950 (5)
∠C4H2*R*3	108	96
Energy (kJ mol^{-1})	−34.7	−3.5
Interaction #2 (intra-layer)		
C5H3···*R*3^{iv}		
H3···*R*3	3.51	3.18
C5···*R*3	4.450 (3)	3.976 (5)
∠C5H3R3	146	143
Energy (kJ mol^{-1})	−18.4	−9.5
Interaction #3 (inter-layer)		
C12H7···*R*3^{v}		
H7···*R*3	3.45	2.70
C12···*R*3	4.090 (3)	3.312 (5)
∠C12H7*R*3	127	123
C6H4···H7Cl2^{vi}		
H4···H7	2.52	2.01
Energy (kJ mol^{-1})	−17.0	−14.7
Interaction #4 (intra-layer)		
C13H8···O1^{vii}		
H8···O1	2.49	2.25
C13···O1	3.396 (2)	3.006 (4)
∠C13H8O1	159	136
Energy (kJ mol^{-1})	−15.1	−11.0
Interaction #5 (intra-layer)		
C3H1···H1C3^{viii}		
H1···H1	2.72	1.96
C4H2···H1C3^{viii}		
H2···H	2.89	2.49
Energy (kJ mol^{-1})	−10.3	−12.9

Symmetry codes: (i) $\frac{1}{2}+x,\frac{1}{2}-y,\frac{1}{2}+z$; (ii) $\frac{3}{2}-x,\frac{1}{2}+y,\frac{1}{2}-z$; (iii) $\frac{3}{2}-x,-\frac{1}{2}+y,\frac{1}{2}-z$; (iv) $-1+x,y,z$; (v) $\frac{5}{2}-x,\frac{1}{2}+y,\frac{1}{2}-z$; (vi) $\frac{1}{2}+x,\frac{3}{2}-y,-\frac{1}{2}+z$; (vii) $2-x,1-y,-z$; (viii) $1-x,1-y,-z$. *R*1 = C2—C3—C4—C5—C6—C7; *R*2 = C1—C2—C7—C8—C9—C14; *R*3 = C9—C10—C11—C12—C13—C14.

lations also yield Mulliken atomic charges, which range from 0.13 to 0.15 e for the H atoms, with H1 and H8 being the most acidic. This is consistent with the formation of chains of molecules which run parallel to the *c* axis, interacting with each other *via* C13H8···O1 contacts (interaction #4 in Table 2: total energy = −15.1 kJ mol^{-1}) which form in pairs across inversion centres (Fig. 5*a*). Chains of molecules interact with each other through CH···π interactions (interaction #2: total energy = −18.4 kJ mol^{-1}) and H···H contacts (interaction #5: total energy = −10.3 kJ mol^{-1}) to form layers which stack along the *b* axis (Fig. 5*b*). The layers interact with one another *via* C11H6···O1 contacts, π interactions and H···H contacts (interactions #1 and #3: total energies = −34.7 and −17.0 kJ mol^{-1}; Figs. 5*b* and *c*). The total energy of the interactions within the layers (intra-layer: # 2, 4 and 5 in Table 2) is −43.8 kJ mol^{-1}, and is slightly less than the total energy of interactions between the layers (inter-layer: # 1 and 3 in Table 2), which is −51.7 kJ mol^{-1}.

A breakdown of the total energy for the contacts is given in Table S3 of the supplementary material. At ambient conditions all five interactions are dominated by the dispersion term, except for #4 (a CH···O contact), where dispersion and Coulombic terms are approximately the same (−11.6 and −12.2 kJ mol^{-1}). The total lattice energy calculated by the PIXEL method at ambient conditions is −146.8 kJ mol^{-1} ($E_{\rm Coul}$ = −47.5 kJ mol^{-1}, $E_{\rm pol}$ = −19.7 kJ mol^{-1}, $E_{\rm disp}$ = −183.8 kJ mol^{-1}, $E_{\rm rep}$ = 104.3 kJ mol^{-1}). PIXEL lattice energies can be validated by comparison with experimental sublimation enthalpies, but to our knowledge there is no literature value for the sublimation enthalpy of bianthrone.

3.3. Compression of bianthrone to 6.5 GPa

The compression of bianthrone is anisotropic (Fig. 6*a*) and the crystal remains in a compressed form of its ambient phase up to 6.5 GPa (Table 1). The path of compression is conveniently visualized in the form of a movie shot along the *c*-axis direction; this movie is available in Quicktime format in the supplementary material.

The greatest degree of compression occurs along the *b* axis, which decreases by 16.5% between ambient pressure and 6.5 GPa. Compression along the *b* axis is substantially greater than along the *a* or *c* axes, which compress by 4.7 and 3.6%. The eigenvector corresponding to the largest eigenvalue of the strain tensor lies along the *b* axis (Fig. 5*a*).

The pressure–volume data for bianthrone were fitted to a Vinet equation-of-state (Vinet *et al.*, 1986, 1987; Angel *et al.*, 2000; Fig. 6*b*) yielding values of the bulk modulus (K_0) and its pressure derivative (K') equal to 8.1 (5) and 8.6 (5) GPa. The value of V_0, the volume at ambient pressure, was fixed at 941.85 Å^3. Molecular solids typically have K_0 < 30 GPa (Angel, 2004) and the following K_0 values are useful for comparison: $Ru_3(CO)_{12}$ (K_0 = 6.6 GPa); alanine (K_0 = 13.6 GPa and K' = 6.7), NaCl (K_0 = 25 GPa), quartz (37 GPa, K' = 6), ceramics (K_0 = 50–300 GPa) and diamond (K_0 = 440 GPa; Funnell *et al.*, 2010; Slebodnick *et al.*, 2004). Softer molecular structures have relatively high values of K', which indicates that a large degree of compression takes place at low pressure.

By-and-large the intramolecular bond distances and angles do not vary significantly with pressure. This observation is supported by the DFT-optimized structures: although intra-

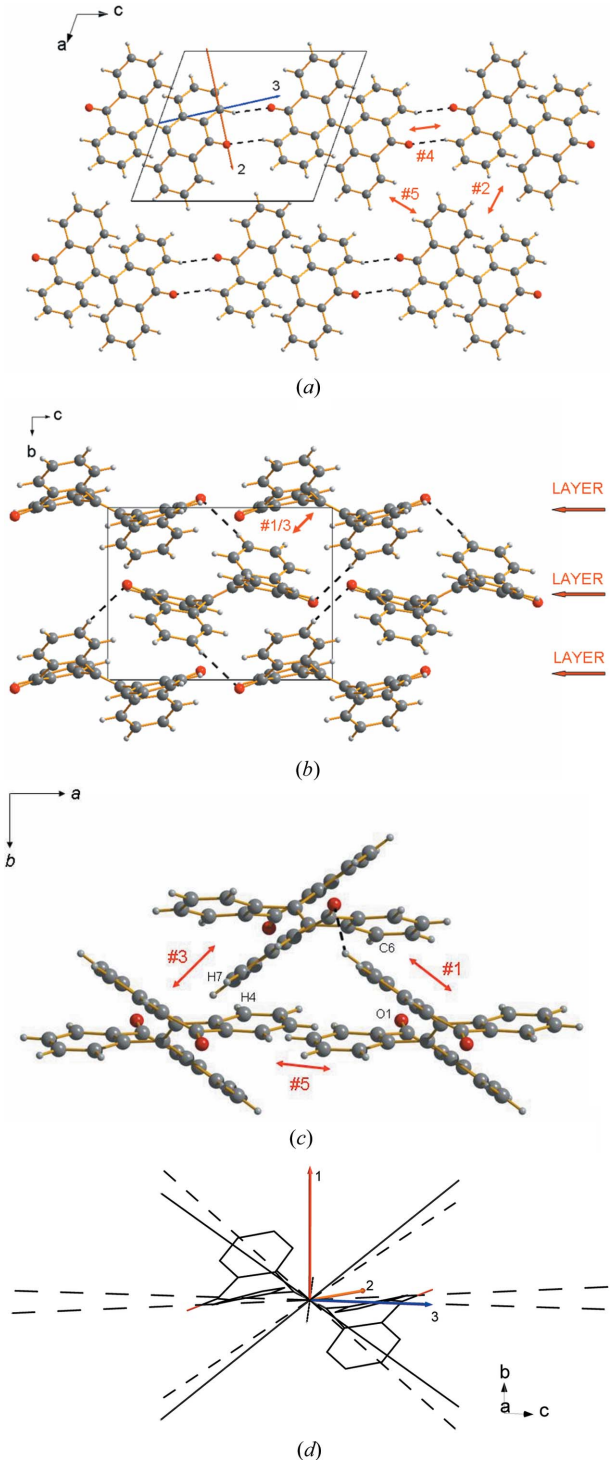

Figure 5
(*a*) One layer of bianthrone molecules viewed along the *b* axis. C13H8···O1 contacts are shown as dashed lines. (*b*) Layers of bianthrone viewed along **a**. (*c*) Layers of bianthrone viewed along **c**. (*d*) The strongest intermolecular interactions in bianthrone shown as solid black lines (35 kJ mol^{-1}) or black dashed lines (10–18 kJ mol^{-1}). Superimposed on the diagrams (*a*) and (*d*) are the principal axes of the strain tensor. The largest component is in red, the smallest blue and the middle in orange. Notice that the largest component avoids the strongest contacts. The red labels #1–#5 represent the PIXEL interactions in Table 2. The molecules involved in interactions #1 and #3 are related by a lattice translation along **a**, and are superimposed in the projection shown in (*b*), but can be more clearly distinguished in (*c*).

molecular bond distances are systematically shorter at 6.5 GPa than at ambient pressure, the differences are too small to be statistically significant when measured experimentally. The exceptions to this are bond distances C1—C2 and C1—C14 formed at the carbonyl group, which shorten by 0.025 and 0.026 Å (DFT) and 0.019 (4) and 0.029 (5) Å (X-ray). The largest difference in bond angle between 6.5 GPa and ambient pressure is seen for C1—C2—C3, which reduced by 1.82 (DFT) and 1.2 (2)° (X-ray). The overall folded shape of the bianthrone molecules remains throughout the compression study, although some of the torsion angles change significantly. The average change in non-H torsion angle between ambient conditions and 6.5 GPa is *ca* 4°, and the largest differences occur in τ(C8′—C8—C9—C10) [44.4 (2)–33.9 (5)°] and τ(C8′—C8—C9—C14) [−137.2 (2) to −147.0 (3)°] corresponding to a flattening of the molecules.

The H···O···O distances in the CH···O contacts (Table 2) are 2.49 and 2.59 Å at ambient pressure and 2.25 and 2.23 Å at 6.5 GPa; the H···ring centroid distances in the CH···π interactions lie between 3.07 and 3.70 Å at ambient pressure and 2.70 and 3.53 Å at 6.5 GPa; the H···H distances lie

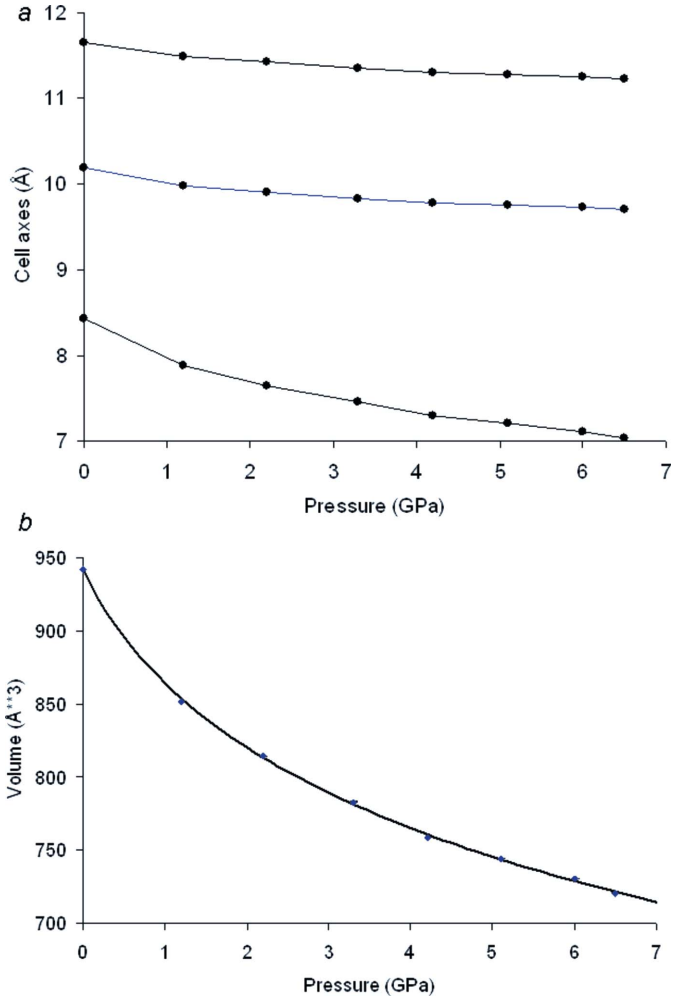

Figure 6
Unit-cell axis lengths and (*b*) unit-cell volume of bianthrone as a function of pressure. The trendline in (*b*) represents the Vinet equation of state with parameters K_0 = 8.1 (5) GPa and K' = 8.6 (5).

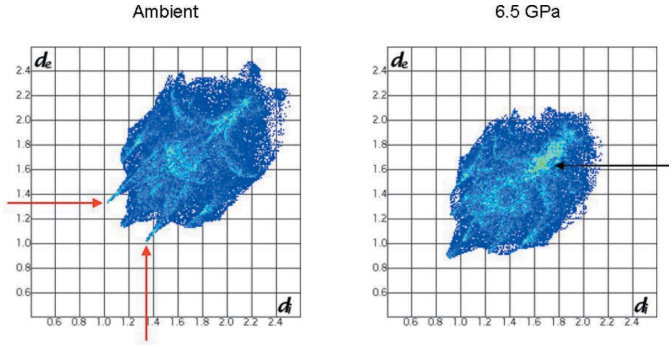

Figure 7
Fingerprint plots for bianthrone at ambient conditions and at 6.5 GPa. Green areas represent an increased frequency of contact distances compared with the blue areas. The red arrows point towards the two 'prongs' which represent H···O distances, and the black arrow points towards an area of C···C distances.

between 2.52 and 2.89 Å at ambient conditions and 1.96 and 2.49 Å at 6.5 GPa. The centroid-to-centroid distance of the $\pi\cdots\pi$ stacking interaction which forms part of interaction #1 decreases by 16.6% upon compression to 6.5 GPa.

These features are summarized effectively in Hirshfeld fingerprint plots (McKinnon *et al.*, 2004) of the structures of bianthrone at ambient pressure and 6.5 GPa (Fig. 7).[2] The two prongs which represent CH···O interactions are prominent at ambient conditions (red arrows) but become masked as a result of the relatively larger contraction in the short H···H contacts at 6.5 GPa. The compressed stacking interactions lead to an increase in the number of distances in the middle of the plots (black arrow), while the disappearance of the diffuse region at high values of (d_i,d_e) points to closing-up of interstitial voids in the structure.

As pressure is increased on bianthrone, the relative magnitudes of the cohesive energy component terms for each interaction remain consistent with those at ambient conditions (Table S3 in the supplementary material); for example, the dispersion component in contacts 1, 2, 3 and 5 still dominates at 6.5 GPa and for contact #4, the Coulombic and dispersion components are effectively equal.

4. Discussion

Bianthrone can exist in two structural forms, one folded, the other twisted (Figs. 1*a* and *b*). The folded form is the more stable, but transition to the twisted form can be promoted either thermochemically or photochemically in solution or by application of pressure in the solid state leading to a colour change from yellow to green. Although the colour change observed in the present single-crystal study is from yellow to red, a combination of the results of visual examination, UV–vis spectroscopy and periodic DFT calculations shows that the same transition to the twisted form had occurred. With a single-crystal sample the transition was limited to the surface of the sample, with the bulk of the crystal remaining in a compressed form of the ambient pressure phase. Complete conversion was achieved with a polycrystalline sample.

The crystal structure of the polymorph containing the twisted form could not be obtained because of extreme strain broadening of the powder diffraction data. We were, however, able to collect single-crystal data which reveal the behaviour of the yellow form of bianthrone as it is compressed. The compression can be understood in terms of the need to compress voids and pack space efficiently, while avoiding compression of the main intermolecular interactions. Fig. 5(*d*)

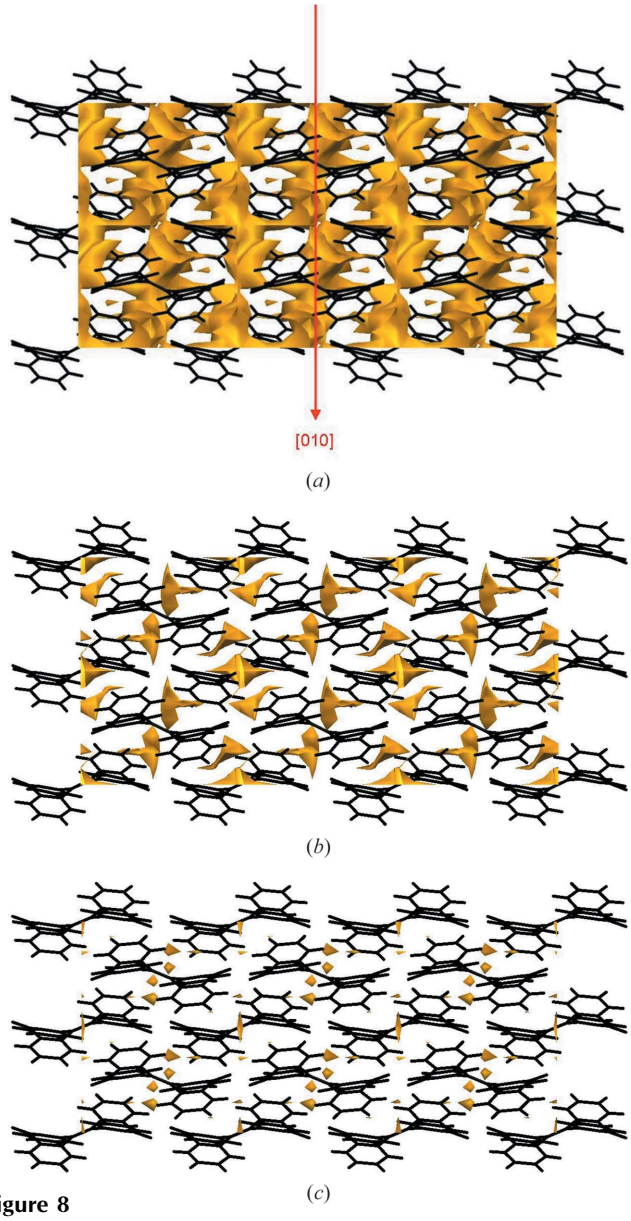

Figure 8
Void diagrams of bianthrone at ambient conditions (*a*) 2.2 GPa (*b*) and 6.5 GPa. The red arrow in (*a*) represents the direction of greatest linear strain throughout the compression study. The view is along the *a* direction and should be compared with Fig. 4(*b*).

[2] Hirshfeld surfaces provide a useful way of looking at the packing environment in a crystal structure. The surface is created by applying the Hirshfeld stockholder partitioning method to divide the crystal into regions in which the electron density of the crystal is dominated by the electron density of a specific molecule. A number of useful properties can be mapped onto the surface including d_e (distances to nearest external atom) and d_i (distances to nearest internal atom) and the electrostatic potential.

shows the principal components of the strain tensor superimposed on the most important intermolecular interactions. The strongest intermolecular interactions are shown as solid black lines (35 kJ mol^{-1}), other interactions falling in the range 10–18 kJ mol^{-1} are shown as dashed lines. It is notable that the largest strain component avoids the strongest contacts. The smallest strain component (in blue, labelled '3') lies approximately along the C13H8$\cdots$O1 contacts (Fig. 5*a*).

Fig. 8(*a*) shows the distribution of voids in the structure of bianthrone at ambient pressure. In bianthrone at ambient pressure voids are distributed between the layers which stack along the *b*-axis direction, and are somewhat elongated along the same direction (Fig. 8*a*). Compression along the *b* direction is an efficient way to reduce the sizes of these voids (Figs. 8*b* and *c*), but as this compression occurs the molecules become flatter in the same direction (see movie), with the torsion angles τ(C8′—C8—C9—C10/14) changing by around 10°.

Fig. 9 shows the total energy of the top five intermolecular interactions in bianthrone as a function of the centroid–centroid distance. Interactions #1, 3 and 4 all show similar behaviour: as pressure is applied the total interaction energies become rapidly more positive. The energy of interaction #2 becomes more negative initially, but this too becomes more positive above 2.2 GPa. Only interaction #5 becomes more stable with pressure, but only slightly. PIXEL calculations do not enable these energy changes to be broken down into atom–atom interaction energies, but it is notable that in contact #1 the distance between atoms C6 and O1 (Fig. 2*c*), which is 3.27 Å at ambient conditions, is 2.69 Å at 6.5 GPa (well within the sum of the van der Waals radii). Similarly, in contact #3 the distance between atoms H7 and H4 (Fig. 2*c*) is 2.52 Å at ambient conditions and 2.01 Å at 6.5 GPa. In the DFT-optimized 6.5 GPa structure, in which the H-atom positions are likely to be more accurate than those derived by X-ray diffraction, this interaction measures 1.806 Å which is very short in the context of other H$\cdots$H contacts in the CSD (Wood *et al.*, 2008).

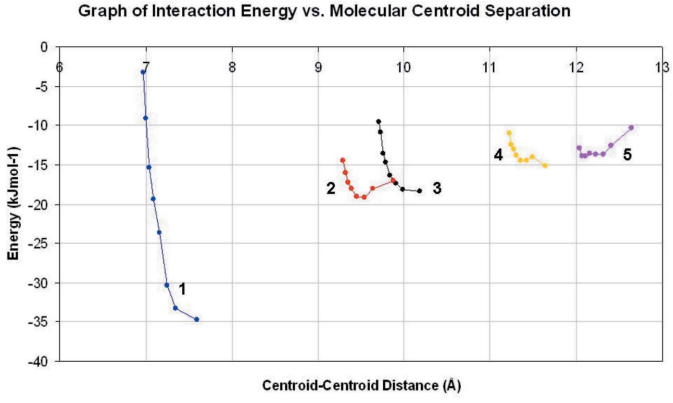

Figure 9
Graph of total interaction energy against the distance between the molecular centroids of the molecules involved in the interaction in bianthrone. The numbers 1–5 refer to the contacts listed in Table 2.

It is clear from Fig. 9 that several intermolecular interactions in bianthrone are driven well into the unstable regions of their potentials at 6.5 GPa. In other structures, *e.g.* salicylaldoxime (Wood *et al.*, 2006), such behaviour has been observed prior to a phase transition, and it is possible that in bianthrone relief of repulsive contacts forms part of the motive for transformation to the twisted form of the compound, although without the crystal structure of this form to compare it is impossible to make a definitive statement.

In high-pressure phase transitions there is always a reduction in volume, leading to a negative $P\Delta V$ contribution to ΔG. As pressure increases this term becomes ever more important, and, as was seen in serine hydrate (Johnstone *et al.*, 2008), transitions can be driven entirely by this term, even at the expense of making the internal energy (U) more positive. In bianthrone, Fanselow & Drickamer (1974) estimated on the basis of variable-temperature measurements of the equilibrium constant between the two forms of bianthrone that at 6 GPa the volume of the twisted form was 0.9 cm^3 mol^{-1} (1.5 Å^3 molecule^{-1}) smaller than the folded form. This would contribute a $P\Delta V$ energy advantage of $\sim$5 kJ mol^{-1} to a crystal composed of the twisted form of the compound at 6 GPa, a substantial figure in the context of polymorphism.

The transition from the folded to the twisted form of bianthrone that occurs with pressure is thus driven by the lower volume of the twisted form, and possibly the relief of strain in the intermolecular interactions which builds as pressure is increased. It would be extremely interesting to grow a crystal of bianthrone directly from solution, although its relatively low solubility in common solvents precluded the use of *in situ* crystallization methods currently in use (Fabbiani *et al.*, 2004).

5. Conclusions

It has been known for decades that bianthrone can exist in two different forms which contain different molecular conformations: one, containing folded molecules (Fig. 1*a*), is yellow; the other, containing twisted molecules (Fig. 1*b*), is green. The transition between the two forms can be accomplished by grinding. In contrast, when a yellow single crystal of bianthrone was placed under hydrostatic compression the sample began to assume a *red* colouration at 3 GPa (Fig. 2). The colour intensifies with pressure, samples appearing black at 8 GPa.

In spite of the differences in colour observed on grinding and hydrostatic compression, high-pressure UV–vis spectroscopy confirmed that the colour change was accompanied by the appearance of the same band previously associated with the twisted conformer. Powder diffraction indicates that the colour change is associated with a polymorphic transition which appears to be complete above 9 GPa. The red colouration is the result of the co-existence of the two forms, the tails of the two absorption bands responsible for the colours of the two forms overlapping in the green region of the spectrum.

Single-crystal diffraction data could be collected up to 6.5 GPa, yielding detailed data on how the yellow form responds to compression. The cell contracts anisotropically, with the greatest decrease in the crystallographic *b* direction, which corresponds to a stacking of layers in the structure. The smallest decrease occurs in a direction corresponding to the strongest CH···O contacts. PIXEL calculations show that as pressure is applied the main intermolecular interactions in the structure become significantly less stable. Previous work had shown that the twisted form of bianthrone has a smaller volume than the folded form, but these results suggest that relief of strained contacts may also play a role in driving the transition.

There is currently substantial interest in polymorphic transitions, reactions and co-crystal formation which can be induced with grinding (Toda, 2007; Friscic & Jones, 2009; Karki *et al.*, 2009). Grinding with a pestle and mortar can produce pressures of up to a few kbar, yet this is enough to induce the transition between the folded and twisted forms of bianthrone, a change which is only observed at pressures of 10 s of kbar in a diamond–anvil cell. This illustrates the important distinction between hydrostatic pressure (as generated in the present experiments) and the non-hydrostatic or shear pressures which are generated on grinding.

We thank EPSRC, The University of Edinburgh and the Cambridge Crystallographic Data Centre for studentship support to RDLJ and STFC, SRS Daresbury Laboratory and Diamond Light Source Ltd for provision of synchrotron beamtime. We also thank Dr Stephen Moggach and Dr Alessandro Prescimone for their help during synchrotron beamtime. We also thank Professor Bruce Hudson (Syracuse University, New York) for drawing our attention to piezochromism in bianthrone.

References

Allen, F. H. (2002). *Acta Cryst.* B**58**, 380–388.
Altomare, A., Cascarano, G., Giacovazzo, C., Guagliardi, A., Burla, M. C., Polidori, G. & Camalli, M. (1994). *J. Appl. Cryst.* **27**, 435.
Angel, R. J. (2002). *EOSFIT*, Version 5.2. Virginia Tech., Blackburg, VA, USA.
Angel, R. J. (2004). *High Pressure Crystallography*. NATO Science Series II, edited by A. Katrusiak & P. F. McMillan, pp. 21–36. Dordrecht: Kluwer Academic Publishers.
Angel, R. J., Downs, R. T. & Finger, L. W. (2000). *Rev. Mineral. Geochem.* **41**, 559–596.
Betteridge, P. W., Carruthers, J. R., Cooper, R. I., Prout, K. & Watkin, D. J. (2003). *J. Appl. Cryst.* **36**, 1487.
Biedermann, P. U., Stezowski, J. J. & Agranat, I. (2006). *Chem. Eur. J.* **12**, 3345–3354.
Blessing, R. H. (1987). *Crystallogr. Rev.* **1**, 3–58.
Brandenburg, K. & Putz, H. (2005). *DIAMOND*. Crystal Impact, Bonn, Germany.
Bruker–Nonius (2006). *SAINT*, Version 7. Bruker AXS Inc., Madison, Wisconsin, USA.
Clark, S. J., Segall, M. D., Pickard, C. J., Hasnip, P. J., Probert, M. J., Refson, K. & Payne, M. C. (2005). *Z. Kristallogr.* **220**, 567–570.
Dawson, A., Allan, D. R., Parsons, S. & Ruf, M. (2004). *J. Appl. Cryst.* **37**, 410–416.
Fabbiani, F. P. A., Allan, D. R., David, W. I. F., Moggach, S. A., Parsons, S. & Pulham, C. R. (2004). *CrystEngComm*, **6**, 504–511.
Fanselow, D. L. & Drickamer, H. G. (1974). *J. Chem. Phys.* **61**, 4567–4574.
Farrugia, L. J. (1999). *J. Appl. Cryst.* **32**, 837–838.
Frisch, M. J. *et al.* (2004). *GAUSSIAN*03, Revision E.01. Gaussian, Inc., Wallington, CT, USA.
Friscic, T. & Jones, W. (2009). *Cryst. Growth Des.* **9**, 1621–1637.
Funnell, N. P., Dawson, A., Francis, D., Lennie, A. R., Marshall, W. G., Moggach, S. A., Warren, J. E. & Parsons, S. (2010). *CrystEngComm*, **12**, 2573–2583.
Gavezzotti, A. (2003). *OPIX*. University of Milano, Milan, Italy.
Gavezzotti, A. (2005). *Struct. Chem.* **220**, 499–510.
Gavezzotti, A. (2007). *Molecular Aggregation: Structure Analysis and Molecular Simulation of Crystals and Liquids*, p. 323. Oxford University Press.
Gould, R. O., Taylor, R. & Thorpe, M. (1995). *PUCKER*. The University of Edinburgh, Scotland.
Hammersley, A. P. (1997). *FIT2D*. Technical Report, ESRF97HA02T. European Synchrotron Radiation Facility, Grenoble, France.
Harnik, E. (1956). *J. Chem. Phys.* **24**, 297–299.
Harnik, E. & Schmidt, G. M. J. (1954). *J. Chem. Soc.* pp. 3295–3302.
Johnstone, R. D. L., Francis, D., Lennie, A. R., Marshall, W. G., Moggach, S. A., Parsons, S., Pidcock, E. & Warren, J. E. (2008). *CrystEngComm*, **10**, 1758–1769.
Karki, S., Friscic, T. & Jones, W. (2009). *CrystEngComm*, **11**, 470–481.
Korenstein, R., Muszkat, K. A. & Sharafy-Ozeri, S. (1973). *J. Am. Chem. Soc.* **95**, 6177.
Kortum, G. (1974). *Ber. Bunsen-Ges. Phys. Chem.* **78**, 391–403.
Macrae, C. F., Bruno, I. J., Chisholm, J. A., Edgington, P. R., McCabe, P., Pidcock, E., Rodriguez-Monge, L., Taylor, R., van de Streek, J. & Wood, P. A. (2008). *J. Appl. Cryst.* **41**, 466–470.
McKinnon, J. J., Spackman, M. A. & Mitchell, A. S. (2004). *Acta Cryst.* B**60**, 627–668.
Merrill, L. & Bassett, W. A. (1974). *Rev. Sci. Instrum.* **45**, 290–294.
Meyer, H. (1909*a*). *Ber. Dtsch. Chem. Ges. B*, **42**, 143–145.
Meyer, H. (1909*b*). *Monatsh. Chem.* **30**, 165–177.
Moggach, S. A., Allan, D. R., Parsons, S. & Warren, J. E. (2008). *J. Appl. Cryst.* **41**, 249–251.
Monkhorst, H. J. & Pack, J. D. (1976). *Phys. Rev. B*, **13**, 5188.
Parsons, S. (2003). *STRAIN*. University of Edinburgh, Scotland.
Parsons, S., Brown, A., Yellowlees, L., Harris, S. & Wood, P. (2004). Private communication (deposition number CCDC 247865). CCDC, Cambridge, England.
Perdew, J. P., Burke, K. & Ernzerhof, M. (1996). *Phys. Rev. Lett.* **77**, 3865–3868.
Piermarini, G. J., Block, S., Barnett, J. D. & Forman, R. A. (1975). *J. Appl. Phys.* **46**, 2774–2780.
Press, W. H., Teukolsky, S. A., Vetterling, W. T. & Flannery, B. P. (1992). *Numerical Recipes in Fortran*, 2nd Ed. Cambridge University Press.
Sheldrick, G. M. (2001). *SHELXTL-XP*, Version 6.01. University of Göttingen, Germany.
Sheldrick, G. M. (2008). *Acta Cryst.* A**64**, 112–122.
Slebodnick, C., Zhao, J., Angel, R., Hanson, B. E., Song, Y., Liu, Z. & Hemley, R. J. (2004). *Inorg. Chem.* **43**, 5245–5252.
Spek, A. L. (2003). *J. Appl. Cryst.* **36**, 7–13.
Toda, F. (2007). *Cryst. Growth Des.* **9**, 149–175.
Vanderbilt, D. (1990). *Phys. Rev. B*, **41**, 7892–7895.
Vinet, P., Ferrante, J., Rose, J. H. & Smith, J. R. (1987). *J. Geophys. Res.* **92**, 9319–9325.
Vinet, P., Ferrante, J., Smith, J. R. & Rose, J. H. (1986). *J. Phys. Solid State Phys.* **19**, L467–L473.
Wasserman, E. & Davies, R. E. (1959). *J. Chem. Phys.* **30**, 1367.
Watkin, D. J., Pearce, L. & Prout, K. (1993). *CAMERON*. Chemical Crystallography Laboratory, University of Oxford, England.

Wolff, S. K., Grimwood, D. J., McKinnon, J. J., Jayatilaka, D. & Spackman, M. A. (2005). *CrystalExplorer*1.5. University of Western Australia.
Wolstenholme, D. J. & Cameron, T. S. (2006). *J. Phys. Chem. A*, **110**, 8970–8978.
Wood, P. A., Forgan, R. S., Henderson, D., Parsons, S., Pidcock, E., Tasker, P. A. & Warren, J. E. (2006). *Acta Cryst.* B**62**, 1099–1111.
Wood, P. A., McKinnon, J. J., Parsons, S., Pidcock, E. & Spackman, M. A. (2008). *CrystEngComm*, **10**, 368–376.